

ELM-limiter interaction in outer gap scan experiments on JET

W.Fundamenski, J.Paley, L.Pickworth, P.Andrew, A.Boboc, J.Conboy, G.F.Matthews,
R.A.Pitts¹, V.Riccardo and JET EFDA contributors

Euratom/UKAEA Fusion Association, Culham Science Centre, Abingdon, OX14 3DB, UK
¹CRPP, Assoc. Euratom-EPFL, CH-1015, Lausanne, Switzerland

Introduction: The interaction of edge localized modes (ELMs), or more accurately of ELM plasma filaments, with the tokamak first wall (divertor and limiter tiles) is one of the critical issues for ITER. Specifically, the heat fluxes deposited on the limiter tiles by the ELM filaments are of great practical importance for the safe operation of ITER.

Experiments: Dedicated experiments designed to measure the radial profiles of the total energy density of Type-I ELM filaments were recently performed on the JET tokamak. In the absence of a main chamber infra-red (IR) system, which is being installed on JET later this year (2005), an indirect method was adopted. The outer wall gap was slowly reduced in the course of the discharge, while the outer divertor strike point was held fixed at the optimal viewing location for the divertor IR camera. By examining the change in deposited power on

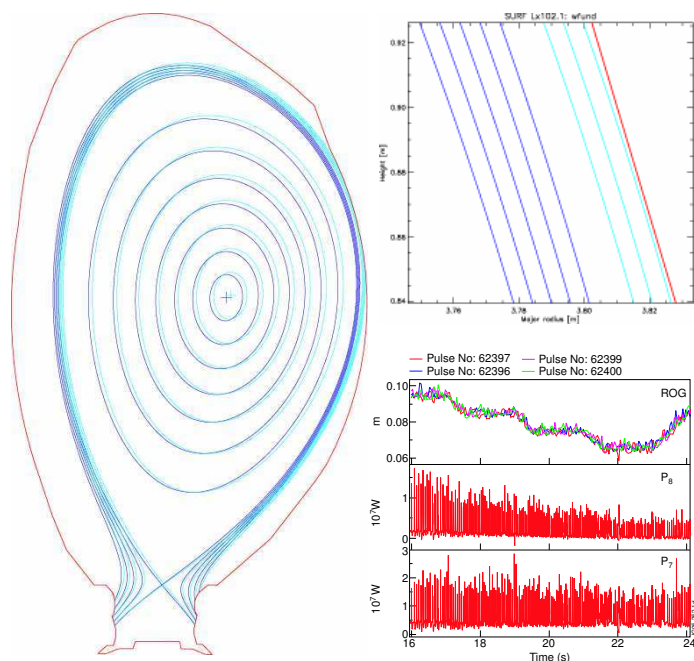


Fig.1: Magnetic equilibria for largest and smallest outer gap (left), magnified region of closest approach to limiter (top) outer gap scan (middle) and IR measured power on outer vertical tiles (7 and 8) for a natural density H-mode.

the outer divertor, while monitoring the fractional drop in the pedestal stored energy, the effective power profile of an average Type-I ELM filament (i.e. the energy e-folding length λ_W^{ELM}) could thus be inferred. A well diagnosed, high clearance plasma configuration extensively used in the past [1,2] (2.5 MA, 2.4 T, $q_{95} \sim 2.6$, 15 MW NBI), was adopted for the outer gap scan experiments. The plasma was positioned such that the outer wall gap or ROG (the radial distance between the separatrix and limiter at the outer mid-plane) had an initial value of 9.5 cm, and was shifted radially outwards in three steps of 1 cm, separated by 2 sec, Fig.1. The position of the separatrix was calculated using the EFIT code with errors estimated at ± 1 cm. For the configurations used here the clearance is smallest near the top of the outboard limiter, which

the outer divertor, while monitoring the fractional drop in the pedestal stored energy, the effective power profile of an average Type-I ELM filament (i.e. the energy e-folding length λ_W^{ELM}) could thus be inferred. A well diagnosed, high clearance plasma configuration extensively used in the past [1,2] (2.5 MA, 2.4 T, $q_{95} \sim 2.6$, 15 MW NBI), was adopted for the outer gap scan experiments. The plasma was positioned such that the outer wall gap or ROG (the radial distance between the

according to EFIT, is reduced from 4 to 1 cm, Fig.1. Since the power width for these plasmas was previously estimated at ~ 5 mm-omp [1], one could expect significant power deposition on the limiter and reduction in power deposition on the divertor, for the case of smallest outer gap. This reduction was in fact observed on the upper tiles (inner: 1 and outer: 8), i.e. in the far-SOL and limiter shadow regions (see below).

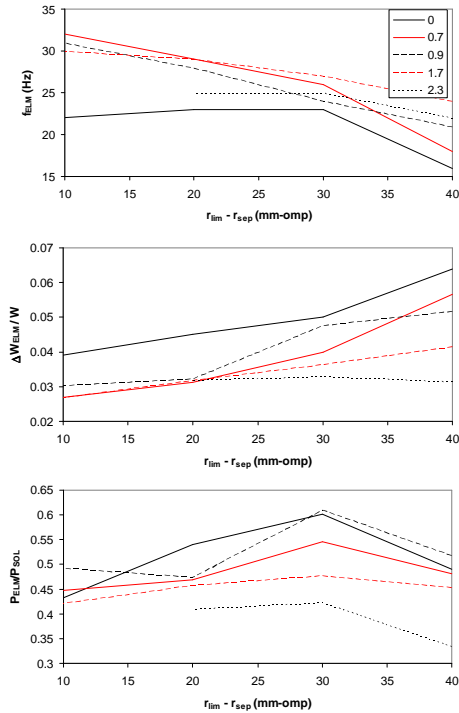


Fig.2: ELM characteristics as a function of clearance and additional gas fuelling.

Six successive discharges of increasing additional fuelling were performed, varying from 0 to 2.3×10^{22} e/s. All shots had similar power entering the SOL, $P_{SOL} \sim 11 - 12$ MW and the line average density increased gradually with additional fuelling. The ELM frequency, f_{ELM} increased with both additional fuelling and reduced outer gap. Since, the ELM power, $P_{ELM} = f_{ELM} \Delta W_{ELM}$ and P_{ELM}/P_{SOL} remained roughly constant, the ELM size, ΔW_{ELM} and the fractional energy drop, $\Delta W_{ELM}/W$ were both reduced with the outer gap, Fig.2. It is noteworthy that impurity levels, Z_{eff} were largest for smallest gap and biggest ELMs. Fast EFIT reconstruction indicates that the separatrix moves inward and down (X-point slightly lower) by up to 1 cm following an ELM. However, there

appears to be little change in strike point position, with only a slight upward movement.

IR/TC analysis: Infra-red thermography data was interpreted using the following analysis

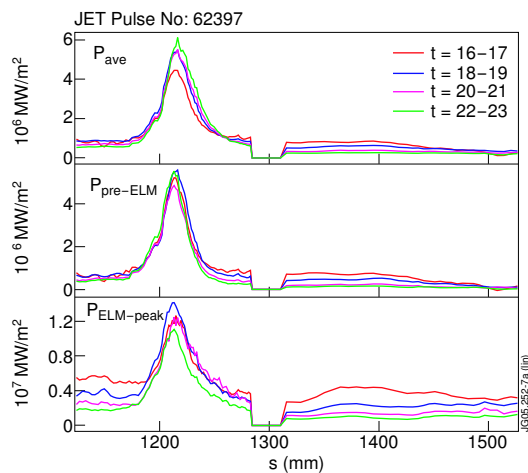


Fig.3: IR measured power profiles on tiles 7 and 8: average (top), pre-ELM (middle) and ELM-peak (bottom) for shot 62397.

algorithm. First, the background radiation was calculated by choosing the outer baffle as the reference location. This background was next subtracted from the observed photon flux. The camera calibration was used to convert the resulting flux into temperatures and the 2D FE Code THEODOR [3] was used to calculate the deposited powers with $\alpha_{inner} = 15$ kW/m²K and $\alpha_{outer} = 150$ kW/m²K on the inner and outer tiles. Finally, the resulting powers were rescaled on a tile by tile basis to match the TC measured energies for the entire shot. The

poloidal profiles of power deposited on outer vertical tiles (7 and 8) as measured by IR thermography are shown in Fig.3 for the lowest density shot, where the ELM-averaged (top), pre-ELM (middle) and ELM-peak (bottom) profiles are plotted. The maximum power at strike point location (tile 7) shows little variation with outer gap. We note the exponential decay with a near-SOL e-folding length of 8 mm-omp, which is roughly the same for inter-ELM and ELM profiles. It is noteworthy that tile 8 power decreases as outer gap is reduced. This was too be expected since, according to EFIT, tile 8 is entirely shadowed by the outboard limiter for the smallest outer gap.

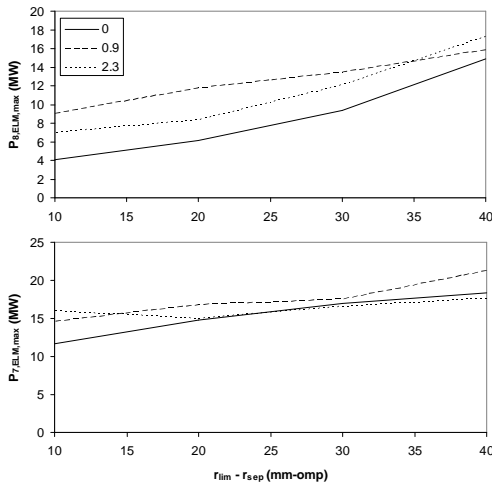


Fig.4: IR measured peak-ELM power to outer vertical tiles (7 and 8) as a function of clearance and gas fuelling.

this reduction, we find the corresponding far-SOL peak ELM filament energy width as $\lambda_{w,max}^{ELM} \sim 24$ mm. These values are in excellent agreement with a recent parallel transport model of ELM filament evolution [4,5], which predicts $\lambda_w^{ELM} \sim 36$ mm and $\lambda_{w,max}^{ELM} \sim 22$

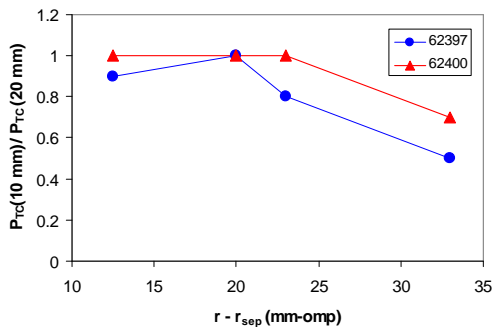


Fig.5: Ratio of TC measured average powers for smallest to next to smallest outer gap, as a function of TC location.

mm, under these conditions, and implies that ions are cooled much slower than electrons in the ELM filaments, such that $T_{i,ELM}/T_{e,ELM} \sim 3$ at the limiter location. The level of agreement is most likely fortuitous, as the error on the experimental values could approach 50%, due to complications in IR analysis. It is therefore encouraging that a similar far-SOL power decay length is obtained from embedded thermocouple (TC) analysis. Although TC sampling is too slow to register individual ELMs, TC data gives a reliable estimate of average deposited energy. The ratio of TC measured power for the smallest gap, $P_{TC}(10)$ with that for the larger gaps, $P_{TC}(20) = P_{TC}(30) = P_{TC}(40)$ (TCs show little change in previous steps) for both the inner and outer target data is shown in

The resulting ELM-averaged (IR) power remains roughly constant on inner and outer lower vertical tiles (3 and 7), but is reduced with outer gap on upper vertical tiles (1 and 8). Similar behaviour is observed for the ELM-peak power, but reduction with outer gap is only observed on tile 8 and is more pronounced than the average power, Fig.4. Taking into account the reduction of ELM size with the outer gap, the far-SOL integral ELM filament energy width is found as $\lambda_w^{ELM} \sim 35$ mm for the lowest density shot. Neglecting

under these conditions, and implies that ions are cooled much slower than electrons in the ELM filaments, such that $T_{i,ELM}/T_{e,ELM} \sim 3$ at the limiter location. The level of agreement is most likely fortuitous, as the error on the experimental values could approach 50%, due to complications in IR analysis. It is therefore encouraging that a similar far-SOL power decay length is obtained from embedded

Fig.5. The reduction is larger for the low density shot and is proportional to the distance away from the separatrix. Neglecting changes in $\Delta W/W$, the corresponding power e-folding length is found as $\lambda_{w,\max}^{\text{ELM}} \sim 22$ mm, in fair agreement with the IR value.

A startling instance of ELM-limiter interaction are the transient displacements of the vacuum vessel with respect to the external supports, as measured by four mechanical sensors

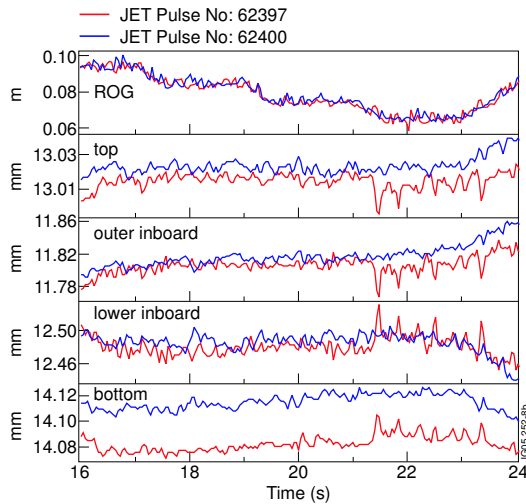


Fig.6: Outer gap and vacuum vessel displacements (mm) measured by mechanical sensors at top, inboard side (twice) and bottom of the machine.

located at the top, inboard (two) and bottom of the vessel. These displacements, which can exceed 50 μm are largest for the smallest outer wall gap and unfuelled H-mode (i.e. largest ELMs), Fig.6. The shape of displacement is consistent with that allowed by the mechanical supports. Although the displacements are clearly linked to $\mathbf{J} \times \mathbf{B}$ forces associated with the transient change in edge current, it is not clear what fraction of this current is provided by the halo-like current flow in the ELM filaments and which by the current change caused by the vertical

stabilisation system. Dedicated experiments in which the latter was disabled indicate that it is likely the dominant cause of the observed vessel displacements, although ELM currents were previously measured at the outer wall using saddle coils on JET [6]. Since vertical stabilisation system would also be active on ITER, the operational implications of such displacements (eg. diagnostic de-calibration, metal fatigue, etc.) should be considered.

Conclusions: Outer gap scan experiments indicate that the far-SOL ELM filament energy density in unfuelled Type-I ELMy H-modes (2.5MA/2.4T, 15MW) on JET evolves with an e-folding length of $\lambda_w^{\text{ELM}} \sim 30$ mm. This result agrees closely with predictions of a recent model of ELM filament evolution based on parallel losses to the divertor targets [4,5].

This work was funded jointly by the United Kingdom Engineering and Physical Sciences Research Council and by the European Communities under the contract of Association between EURATOM and UKAEA. The views and opinions expressed herein do not necessarily reflect those of the European Commission. This work was carried out within the framework of the European Fusion Development Agreement.

[1] W.Fundamenski et al., *Nuclear Fusion* (2005), in press. [2] W.Fundamenski et al., *Plasma Phys. Control. Fusion*, **46** (2004) 233. [3] A.Herrmann et al., *Plasma Phys. Control. Fusion*, **37** (1995) 17. [4] W.Fundamenski, R.A.Pitts et al., submitted to *Plasma Phys. Contr. Fusion* (2005). [5] R.A.Pitts, W.Fundamenski et al., submitted to *Nuclear Fusion* (2005). [6] D.Testa et al, *Plasma Phys. Control. Fusion*, **47** (2005) 733.